

Algebraic Cutting Equations

Damiano Anselmi

Dipartimento di Fisica “Enrico Fermi”, Università di Pisa,

Largo B. Pontecorvo 3, 56127 Pisa, Italy

and INFN, Sezione di Pisa,

Largo B. Pontecorvo 3, 56127 Pisa, Italy

damiano.anselmi@unipi.it

Abstract

The cutting equations are diagrammatic identities that are used to prove perturbative unitarity in quantum field theory. In this paper, we derive algebraic, upgraded versions of them. Differently from the diagrammatic versions, the algebraic identities also holds for propagators with arbitrary, nonvanishing widths. In particular, the cut propagators do not need to vanish off shell. The new approach provides a framework to address unsolved problems of perturbative quantum field theory and a tool to investigate perturbative unitarity in higher-derivative theories that are relevant to the problem of quantum gravity, such as the Lee-Wick models and the fakeon models.

1 Introduction

Perturbative unitarity in quantum field theory is the statement that the scattering matrix S is unitary at the perturbative level. This property can be rephrased as a set of identities obeyed by the scattering amplitudes. At the diagrammatic level, it amounts to a set of *cutting equations* [1], which involve a diagram G together with the variants obtained by cutting G in various ways. In this paper, we show that perturbative unitarity can be conceptually reduced to a set of polynomial equations, which we call *algebraic cutting equations*. They are actually more general than what is strictly needed for the proof of perturbative unitarity, which is why we think that they deserve consideration on their own as mathematical properties.

The usual proof of perturbative unitarity [1, 2, 3] proceeds in four steps, which are the derivations of: (i) a diagrammatic equation in coordinate space known as *the largest time equation*, (ii) the cutting equations properly known (henceforth called *diagrammatic cutting equations*, to distinguish them from the algebraic ones), (iii) the pseudounitariness equation, and (iv) the unitarity equation $SS^\dagger = 1$. In this paper, we concentrate on a new, algebraic approach that allows us to jump directly to point (ii). We will not have much to say about the other steps just mentioned, which remain unmodified.

In particular, the projection (iii) \rightarrow (iv) of the pseudounitariness equation onto the unitarity equation is necessary only in the presence of local symmetries. Its role is to show that the temporal and longitudinal components of the gauge fields are compensated by the Faddeev-Popov ghosts. The projection can be handled with the methods of refs. [2] and [3] in gauge theories and those of ref. [4] in gauge theories and gravity. The implication (ii) \rightarrow (iii) is straightforward, since the pseudounitariness equation is just a collection of the cutting equations. The implication (i) \rightarrow (ii) follows from the Fourier transform of the largest time equation plus the requirement that positive energies propagate forward in time and negative energies propagate backward in time. In the approach we offer here, it is a particular case of the general theorem we prove.

In this paper, we replace the step (i) with a set of algebraic identities that allow us to gain a deeper understanding into the mathematical aspects of perturbative unitarity, and make various manipulations more efficiently. Moreover, the algebraic cutting equations are more general than the usual ones. Indeed, they also hold for arbitrary, nonvanishing widths, since the cut propagators do not need to be distributions that are supported only on shell.

The basic concept we need to build the identities is the concept of *polar* number, which is a variable equipped with a *polarity*. By convention, the polarities are denoted by $+$ and $-$. The polarity is an abstract marking that allows us to divide the set of variables we

use into two subsets: the subset made of the variables with positive polarity and the subset made of the variables with negative polarity. In typical applications, the polar numbers have complex values and the positive/negative polarity can denote their locations inside/outside some closed curve γ on the complex plane or the Riemann sphere. If the polar number is a function of another variable (typically an energy E) and has a singularity for a specific value of E , then the polarity may refer to the location of the singularity inside/outside a closed curve γ .

Given an oriented Feynman diagram G , we give rules to associate one polar number with each internal leg. The product of such polar numbers is called polar monomial. A polarized monomial is a polar monomial where at least one loop is polarized, that is to say each leg of the loop is associated with a polar number whose polarity agrees with the leg orientation. The theorem we prove states that certain polynomials of polar numbers are equal to sums of polarized monomials.

In the applications to physics, the legs of the diagrams are oriented according to energy flows. The polar numbers are “half propagators” (the propagator being the sum of two polar numbers). They depend on a momentum and have a pole for some complex value of the energy. The polarity is positive or negative according to whether the pole is located below or above the real axis of the complex energy plane. The theorem singles out the polarized monomials, which do not contribute to the diagrammatic cutting equations. The reason is that polarized loops give zero when they are integrated on the loop momentum. The algebraic identities thus lead to the diagrammatic cutting equations in a straightforward way.

The approach of this paper offers a clearer understanding of perturbative unitarity, by uncovering its purely algebraic aspects. As we show in section 8, it also helps organizing computations in more practical ways. Moreover, the generalized versions that hold for arbitrary widths allow us to upgrade the formulation of unitarity to include the effects of radiative corrections, which typically generate nonvanishing widths at one and higher loops. Several aspects of this inclusion have yet to be clarified [5].

Finally, the algebraic cutting equations provide the best framework to investigate perturbative unitarity in theories that have not been reached so far by the standard techniques. Examples are the Lee-Wick models [6], which do involve propagators with nonvanishing widths. They are higher-derivative theories of a special class that are claimed to reconcile renormalizability with unitarity. The Lee-Wick models have been studied in a variety of contexts [7] and are expected to have important implications for quantum gravity [8, 9]. They have been reformulated as nonanalytically Wick rotated Euclidean theories in ref. [10]

and their unitarity has been proved at one loop in ref. [11]. They admit important generalizations where the would-be ghosts are turned into “fakeons”, i.e. fake degrees of freedom, by means of a new quantization prescription [9]. Using the algebraic cutting equations, a proof of unitarity to all orders has been recently provided in ref. [12] for all the theories that contain fakeons and physical degrees of freedom.

The paper is organized as follows. In section 2 we collect the basic definitions. In section 3 we state the main theorem, which we prove in section 4. In section 5 we give a number of examples. Specifically, we use the algebraic identities to derive the diagrammatic cutting equations of the bubble and triangle diagrams at one loop and the chestnut diagram at two loops. We include the algebraic identities of other diagrams, up to three loops. In section 6 we use the identities to prove the perturbative unitarity of ordinary quantum field theories. In section 7 we discuss some symmetries of the algebraic cutting equations. Section 8 contains the conclusions, with emphasis on the virtues of the algebraic approach with respect to the usual approach.

2 Basic definitions

In this section we collect the basic definitions that are necessary to state the main theorem.

A diagram is a set of vertices connected by lines. The lines of a diagram will be called *legs* henceforth. The diagrams we consider do not need to be planar or connected. The vertices can be the endpoints of any number of legs, including one or two. The vertices that are attached to a unique leg are called external. The legs they are attached to are also called external. The other vertices and legs are called internal. From now on, we drop the external vertices and whenever we talk about vertices we mean the internal ones.

Equip the internal legs of the diagrams with orientations. The definition of oriented leg is self evident. Two legs are called adjacent if they have a vertex in common. Two adjacent legs are said to have coherent orientations if the orientation of one leg points to the vertex in common and the orientation of the other leg points away from the vertex in common.

Definition 1 *Given a diagram, a curve is a sequence $\{\ell_1, \dots, \ell_n\}$ of legs ℓ_i , such that each ℓ_i with $i > 1$ is adjacent to ℓ_{i-1} . A loop is a closed curve, i.e. a curve $\{\ell_1, \dots, \ell_n\}$ such that ℓ_1 is adjacent to ℓ_n . A curve is minimal if it contains no loop. A loop is minimal if it contains no loop apart from itself.*

An example of nonminimal loop is a loop that looks like an “8”.

Definition 2 *A curve or a loop are oriented if the orientations of all their legs are coherent.*

Assume that G is connected and has I internal legs and V vertices. Pick I independent real numbers E_i , $i = 1, \dots, I$, and call them “energies”. Assign an energy to each internal leg and zero energy to each external leg. Use the orientation of a leg to define the orientation of the flow of its energy. Then, impose the energy conservation at each vertex. This is the requirement that the total energy flowing into the vertex must be equal to the total energy flowing out of the vertex. The independent conservation conditions are $V - 1$, because the energies flowing into the diagram and out of it are zero by assumption. Due to this, the energy is automatically conserved in the last vertex, once it is conserved in every other vertex. Energy conservation leaves us with $I - V + 1 \equiv L$ arbitrary independent energies e_1, \dots, e_L .

Proposition 1 *It is possible to arrange the leg orientations and the energies e_1, \dots, e_L , so that the flow of each energy defines an oriented minimal loop in G and each leg is associated with a linear combination of energies e_1, \dots, e_L with coefficients 0 or 1.*

Proof. To see this, start from the diagram G , with no leg orientations and zero energy in every leg. Assume, for the time being, that G is one-particle irreducible. Consider a minimal loop γ_1 in G . Arrange the orientations of the γ_1 legs so that they are coherent and add the energy e_1 to each of its legs. So doing, the loop γ_1 becomes oriented. If $L = 1$, the construction stops here.

Otherwise, since G is one-particle irreducible, there must exist a pair $v^{(a)}, v^{(b)}$ of γ_1 vertices that are connected by a minimal curve Γ_{ab} which has no legs and no other vertex in common with γ_1 . We distinguish two cases: $v^{(a)} \neq v^{(b)}$ and $v^{(a)} = v^{(b)}$. If $v^{(a)} \neq v^{(b)}$, $v^{(a)}$ and $v^{(b)}$ are connected both by Γ_{ab} and by two portions Δ_{ab} and Δ'_{ab} of γ_1 . Pick the portion of your choice, say Δ_{ab} . The union $\Gamma_{ab} \cup \Delta_{ab}$ defines a minimal loop γ_2 . The orientation of Δ_{ab} can be extended coherently to Γ_{ab} , to define the orientation of γ_2 . Once this is done, add the energy e_2 to each leg of γ_2 . If $v^{(a)} = v^{(b)}$, just pick Γ_{ab} as the loop γ_2 and orient it in the way you like. Then add e_2 to each of its legs. If $L = 2$, the construction stops here.

Observe that any distinct vertices $v^{(c)}$ and $v^{(d)}$ of $\gamma_1 \cup \gamma_2$ are connected by an oriented minimal curve Δ_{cd} contained in $\gamma_1 \cup \gamma_2$: if they both belong to γ_1 or γ_2 , this fact is obvious. If $v^{(c)}$ belongs to γ_1 and $v^{(d)}$ belongs to γ_2 , it is sufficient to move along γ_1 (following the γ_1 orientation) from $v^{(c)}$ to the first intersection between γ_1 and γ_2 , then continue to $v^{(d)}$ along the portion of γ_2 that has a coherent orientation. Clearly, such a Δ_{cd} is a minimal curve.

If $L > 2$, there must exist a pair of vertices $v^{(c)}$ and $v^{(d)}$ of $\gamma_1 \cup \gamma_2$ that are connected by a minimal curve Γ_{cd} that has no legs and no other vertex in common with $\gamma_1 \cup \gamma_2$. If $v^{(c)} \neq v^{(d)}$, by the property shown above they are also connected by an oriented minimal

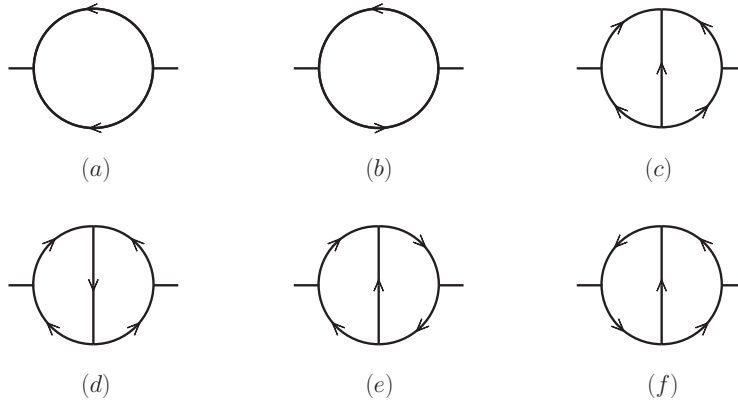


Figure 1: Orientations of diagrams

curve Δ_{cd} contained in $\gamma_1 \cup \gamma_2$. The union $\Gamma_{cd} \cup \Delta_{cd}$ of the two curves defines the third minimal loop γ_3 , which becomes oriented after the orientation of Δ_{ab} is coherently extended to the whole loop. Finally, the energy e_3 is added to all the legs of γ_3 . If $v^{(c)} = v^{(d)}$, just pick Γ_{cd} as γ_3 , orient it in the way you like and add e_3 to each of its legs. If $L = 3$, the construction stops here.

Again, any pair of distinct vertices that belong to the union $\gamma_1 \cup \gamma_2 \cup \gamma_3$ are connected by an oriented curve contained in $\gamma_1 \cup \gamma_2 \cup \gamma_3$, which we can choose to be minimal. This allows us to iterate the construction for $L > 2$.

It is also straightforward to extend the assignments to the one-particle reducible diagrams as well as the disconnected diagrams. This concludes the proof. \square

Definition 3 *A diagram is oriented if its leg orientations are compatible with the construction of proposition 1. Otherwise, the diagram is jammed.*

We call e_1, \dots, e_L *loop energies*. A diagram may admit various orientations, which give equivalent polynomial identities. In fig. 1 we show various examples. The diagrams (a) and (c) are jammed, while (b), (d), (e) and (f) are oriented. In particular, (d), (e) and (f) are different orientations of the same diagram. A diagram has precisely L oriented minimal loops. For example, (d), (e) and (f) have two oriented minimal loops.

3 The theorem

In this section we state the theorem, leaving its proof to the next section.



Figure 2: Propagators

Let G denote an oriented diagram and ℓ_1, \dots, ℓ_I its internal legs. Let ν_a , $a = 1, \dots, V$, label the vertices of the diagram. When we want to specify that the orientation of the i th leg points from, say, the vertex ν_a to the vertex ν_b , we denote it by $(\nu_a \ell_i \nu_b)$.

Build variants G_M of G by marking any number of vertices. We denote the marked vertices by $\hat{\nu}_a$. The marked diagrams have legs of types $(\nu_a \ell_i \hat{\nu}_b)$, $(\hat{\nu}_a \ell_i \nu_b)$ and $(\hat{\nu}_a \ell_i \hat{\nu}_b)$, besides those of type $(\nu_a \ell_i \nu_b)$, the leg orientation pointing from a to b .

A *polar* number is a variable equipped with a *polarity*, denoted by $+$ or $-$. Let $\{\sigma_i^+, \tau_i^+, \sigma_i^-, \tau_i^-\}$, $i = 1, \dots, I$, denote I quartets of polar numbers. Each quartet is associated with a leg of the diagram and is the union of a pair σ_i^+, τ_i^+ of variables with positive polarities and a pair σ_i^-, τ_i^- of variables with negative polarities.

Define the *propagators*

$$z_i = \sigma_i^+ + \sigma_i^-, \quad w_i = \tau_i^+ + \tau_i^-, \quad u_i = \sigma_i^+ + \tau_i^-, \quad v_i = \sigma_i^- + \tau_i^+. \quad (3.1)$$

Determine the *value* P_M of the diagram G_M by means of the following ‘‘Feynman’’ rules. Assign the value one to each unmarked vertex and the value -1 to each marked one. Associate propagators with the legs of G_M as follows:

$$(\nu \ell_i \nu') \rightarrow z_i, \quad (\hat{\nu} \ell_i \hat{\nu}') \rightarrow w_i, \quad (\nu \ell_i \hat{\nu}') \rightarrow u_i, \quad (\hat{\nu} \ell_i \nu') \rightarrow v_i. \quad (3.2)$$

Graphically, we denote the marked vertices by means of a dot, so the propagators are those shown in fig. 2. Then, P_M is the polynomial

$$P_M = (-1)^m \prod_{i=1}^I p_{Mi}, \quad (3.3)$$

where p_{Mi} denotes the propagator of the i th leg ℓ_i , assigned according to the scheme (3.2), and m is the number of marked vertices.

For example, the polynomials associated with the marked diagrams of fig. 3 are

$$z_1 z_2, \quad w_1 w_2, \quad -u_1 v_2, \quad -v_1 u_2, \quad (3.4)$$

respectively.

The set of marked diagrams includes the diagram G itself, where all the vertices are unmarked, as well as the diagram \bar{G} where all the vertices are marked. The polynomials P and \bar{P} associated with G and \bar{G} are

$$P = \prod_{i=1}^I z_i, \quad \bar{P} = (-1)^V \prod_{i=1}^I w_i,$$

respectively.

The theorem is about the sum of the polynomials P_M on all the ways M to mark the diagram G . Writing z, w, u and v as sums of polar numbers, according to formula (3.1), we can expand the sum of P_M as a sum of *polar monomials*. A polar monomial is the product of one polar number of the set $\{\sigma_i^+, \tau_i^+, \sigma_i^-, \tau_i^-\}$ for each leg l_i . A polar curve, loop or diagram is a curve, loop or diagram whose legs are equipped with polar numbers.

Examples of polar monomials for the diagram G of fig. 3 are

$$\sigma_1^+ \sigma_2^+, \quad \sigma_1^- \tau_2^-, \quad \sigma_1^+ \sigma_2^-, \quad \sigma_1^+ \tau_2^-, \quad \sigma_1^- \tau_2^+, \quad (3.5)$$

etc.

Definition 4 A *polarized loop* is a polar loop where adjacent legs of coherent (opposite) orientations carry polar numbers of coherent (opposite) polarities.

In particular, an oriented polar loop is polarized if all its legs carry polar numbers of the same polarity. Instead, a polarized nonoriented loop is such that the leg polarity flips if and only if the orientation flips.

Definition 5 A *polarized monomial* is a polar monomial, associated with a diagram G , where at least one loop is polarized.

Consider, for example, the diagrams of fig. 4. The oriented loops of the first diagram are 123 and 345, while 1254 is a nonoriented loop. If we equip such loops with the polar monomials $\sigma_1^+ \sigma_2^+ \tau_3^+$, $\sigma_3^- \tau_4^- \tau_5^-$ and $\sigma_1^+ \sigma_2^+ \sigma_4^- \tau_5^-$, respectively, we obtain polarized loops. Examples of polarized monomials are $\sigma_1^+ \sigma_2^+ \tau_3^+ \sigma_4^+ \tau_5^-$ and $\sigma_1^+ \sigma_2^+ \sigma_3^- \tau_4^- \tau_5^-$. Examples of polarized loops



Figure 3: Simple marked diagrams

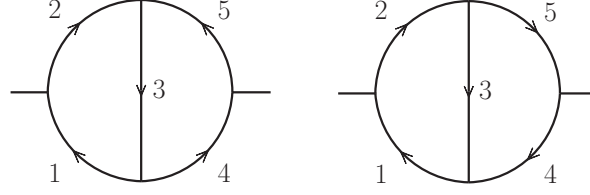


Figure 4: Two-loop oriented diagrams

for the second diagram of fig. 4 are 123 with the monomial $\sigma_1^+ \sigma_2^+ \tau_3^+$, 1254 with $\sigma_1^+ \sigma_2^+ \tau_4^+ \sigma_5^+$ and 345 with $\sigma_3^+ \sigma_4^- \tau_5^-$.

Here is the main theorem of this paper:

Theorem 1 *given a diagram G , the identity*

$$\sum_{\text{markings } M} P_M = \mathcal{P}_G \quad (3.6)$$

holds, where \mathcal{P}_G is a sum of polarized monomials.

We can condense the theorem by saying that the sum of the marked diagrams is equal to a sum of polarized diagrams.

For example, if we sum the polynomials (3.4), we can easily check the identity

$$z_1 z_2 + w_1 w_2 - u_1 v_2 - v_1 u_2 = (\sigma_1^+ - \tau_1^+)(\sigma_2^+ - \tau_2^+) + (\sigma_1^- - \tau_1^-)(\sigma_2^- - \tau_2^-). \quad (3.7)$$

Note that the right-hand side is a sum of polarized monomials. More examples are given in section 5.

At the tree level, we have $\mathcal{P}_G = 0$. At one loop, we have the general formula

$$\mathcal{P}_G = \prod_{i=1}^I (\sigma_i^+ - \tau_i^+) + \prod_{i=1}^I (\sigma_i^- - \tau_i^-), \quad (3.8)$$

which we leave without proof, since it is not crucial for the rest of the discussion.

We can assume that the diagram G does not contain tadpoles, i.e. loops made of a single leg that begins and ends at the same vertex. Indeed, if G contains tadpoles, the theorem is trivial, since a tadpole is an oriented loop and can obviously be written as the sum of two contributions, each being a polar number, which is polarized by definition. Moreover, we can also assume that G is connected, since the theorem extends to disconnected diagrams in an obvious way, once it is proved for connected diagrams. Finally, we can assume $V > 1$, since a diagram with a single vertex has no internal leg (in which case the theorem is obvious) or is a tadpole.

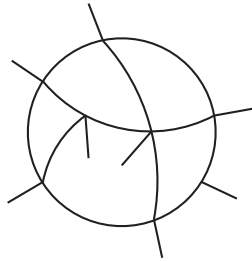


Figure 5: Diagram with one external leg for each vertex

4 Proof of the theorem

In this section we prove the theorem. Since formula (3.6) is a polynomial identity, if we prove it for polar numbers belonging to open sets of the complex plane, we automatically prove it for arbitrary polar numbers. Thus, with no loss of generality, we can assume that the signs of the imaginary parts of the polar numbers $\sigma_i^+, \tau_i^+, \sigma_i^-, \tau_i^-$ coincide with their polarities.

Let G denote an oriented connected diagram with I internal legs, V vertices, $L = I - V + 1$ loops and no tadpoles. Denote the internal legs by ℓ_i , $i = 1, \dots, I$, and the vertices by ν_a , $a = 1, \dots, V$. We can assume $V > 1$ and equip G with loop energies e_1, \dots, e_L in the way specified by proposition 1.

If more external legs are attached to the same vertex, drop all of them but one. If no external leg is attached to a vertex, add one. So doing, each vertex is attached to one external leg and the diagram G becomes a figure like fig. 5. Note that some external legs are drawn inside the diagram, for no particular reason other than aesthetics. They could be prolonged at will by crossing over the internal legs, since Feynman diagrams need not be planar.

Assign propagators identically equal to one to the external legs. Then, equip each external leg but the last one with an independent energy \mathcal{E}_a , $a = 1, \dots, V - 1$, that flows into the diagram. By the conservation of energy, the external leg attached to the last vertex ν_V has energy $\sum_{a=1}^{V-1} \mathcal{E}_a$ flowing out of the diagram.

By the argument of section 2, if G is one-particle irreducible, each pair of vertices $\{\nu_a, \nu_V\}$, $a = 1, \dots, V - 1$, is connected by a minimal curve Γ_a in G that is oriented from ν_a to ν_V . This property can be easily extended to any connected diagram G . If G is one-particle reducible, it can be viewed as a tree of one-particle irreducible subdiagrams G_A , $A = 1, \dots, N$, and single (nonoriented) lines ℓ_A , $A = 1, \dots, N - 1$, connecting pairs of

G_A 's. Equip ℓ_A with the orientation that flows towards the subdiagram \tilde{G}_A that contains ν_V . Then, given a pair of vertices $\{\nu_a, \nu_V\}$, $a = 1, \dots, V-1$, it is possible to connect them through a minimal curve Γ_a that is oriented from ν_a to ν_V and is equal to the union of a set of oriented minimal curves $\Gamma'_A \subset G_A$ and lines ℓ_A .

Add the energy \mathcal{E}_a to all the legs of Γ_a . Let E_i denote the energy of the i th internal leg ℓ_i . By proposition 1 and the construction just described, E_i is a linear combination of the loop energies e_1, \dots, e_L and the external energies $\mathcal{E}_1, \dots, \mathcal{E}_{V-1}$, with coefficients 0 or 1.

Define new polar numbers ζ_i^\pm and ξ_i^\pm as

$$\sigma_i^\pm = E_i - (\zeta_i^\pm)^{-1}, \quad \tau_i^\pm = E_i - (\xi_i^\pm)^{-1}. \quad (4.1)$$

Their polarities, specified by the superscripts $+$ and $-$, coincide with the signs of their imaginary parts. We have

$$\sigma_i^\pm(E_i) = \frac{1}{E_i - \zeta_i^\pm}, \quad \tau_i^\pm(E_i) = \frac{1}{E_i - \xi_i^\pm}. \quad (4.2)$$

For a while, we keep ζ_i^\pm and ξ_i^\pm fixed and treat σ_i^\pm and τ_i^\pm as functions of the energies. In some intermediate steps we integrate over the loop energies. Then, we undo the integral to recover properties that hold at arbitrary energies. This is the strategy that leads to the proof of the theorem.

Now, pick a marked diagram G_M , take formula (3.3), implement the replacements (4.2) and integrate each loop energy e_j along the real axis with the measure $de_j/(2\pi)$. This defines the value of G_M in energy space, which is

$$G_M(\mathcal{E}_1, \dots, \mathcal{E}_{V-1}) = (-1)^m \int \prod_{i=1}^I P_{M_i}(E_i) \prod_{j=1}^L \frac{de_j}{2\pi}. \quad (4.3)$$

This integral is overall convergent, because it is well behaved at infinity and no pole sits on the real axis. As far as the overall behavior at infinity is concerned, observe that each polar number decreases like $1/e$, where e collectively denotes the loop energies, so the overall behavior of P_M is $1/e^I$, which falls off fast enough, since $V > 1$ implies $I = L+V-1 \geq L+1$. Moreover, every subintegral is overall convergent for a similar reason. Incidentally, the reason why we cannot treat diagrams that contain tadpoles is that they do not satisfy these conditions.

We move to the coordinate versions of the diagrams, by taking their Fourier transforms. The Fourier transforms of the polar numbers σ_j^\pm and τ_j^\pm are

$$\tilde{\sigma}_j^\pm(t_j) = \int_{-\infty}^{+\infty} \frac{dE_j}{2\pi} \frac{e^{iE_j t_j}}{E_j - \zeta_j^\pm} = \pm i\theta(\pm t_j) e^{it_j \zeta_j^\pm}, \quad \tilde{\tau}_j^\pm(t_j) = \pm i\theta(\pm t_j) e^{it_j \xi_j^\pm}.$$

Familiar knowledge of quantum field theory tells us that the coordinate version \tilde{G}_M of (4.3) [multiplied by the distribution $(2\pi)\delta(\mathcal{E}_1 + \mathcal{E}_2 + \dots + \mathcal{E}_V)$, which imposes the overall energy conservation, where \mathcal{E}_V is an independent energy] is the product of the propagators in coordinate space, times the values of the vertices, integrated over the locations μ_a of the vertices, i.e.

$$\tilde{G}_M(t_1, \dots, t_V) = (-1)^m \int \prod_{a=1}^V [d\mu_a \delta(t_a - \mu_a)] \prod_{j=1}^I \tilde{p}_{Mj}(\mu_{a_j} - \mu_{b_j}).$$

Here $\tilde{p}_{Mj}(\mu_{a_j} - \mu_{b_j})$ denotes the Fourier transform of the propagator p_{Mj} associated with the line ℓ_j and μ_{a_j}, μ_{b_j} are the time coordinates of the ℓ_j endpoints, ordered so that the ℓ_j orientation points from the vertex of time μ_{a_j} to the vertex of time μ_{b_j} . The delta functions are the Fourier transforms of the propagators of the external legs (which are identically one in energy space).

The μ integrals are straightforward, so we just get

$$\tilde{G}_M(t_1, \dots, t_V) = (-1)^m \prod_{j=1}^I \tilde{p}_{Mj}(t_{a_j} - t_{b_j}).$$

We can formulate the Feynman rules of the diagrams in coordinate space as follows. As usual, the unmarked vertices are equal to one and the marked vertices are equal to -1 . The propagators $\tilde{p}_{Mj}(t_a - t_b)$ are assigned according to the scheme

$$\begin{aligned} (\nu_a \ell_j \nu_b) &\rightarrow z_j = \sigma_j^+ + \sigma_j^- \rightarrow i\theta(t_{ab})e^{it_{ab}\zeta_j^+} - i\theta(-t_{ab})e^{it_{ab}\zeta_j^-}, \\ (\nu_a \ell_j \hat{\nu}_b) &\rightarrow u_j = \sigma_j^+ + \tau_j^- \rightarrow i\theta(t_{ab})e^{it_{ab}\zeta_j^+} - i\theta(-t_{ab})e^{it_{ab}\xi_j^-}, \\ (\hat{\nu}_a \ell_j \nu_b) &\rightarrow v_j = \sigma_j^- + \tau_j^+ \rightarrow i\theta(t_{ab})e^{it_{ab}\xi_j^+} - i\theta(-t_{ab})e^{it_{ab}\zeta_j^-}, \\ (\hat{\nu}_a \ell_j \hat{\nu}_b) &\rightarrow w_j = \tau_j^+ + \tau_j^- \rightarrow i\theta(t_{ab})e^{it_{ab}\xi_j^+} - i\theta(-t_{ab})e^{it_{ab}\xi_j^-}, \end{aligned} \quad (4.4)$$

where $t_{ab} = t_a - t_b$ and t_a denotes the time coordinate of the vertex ν_a .

Now we show that

Lemma 1 *the identity*

$$\sum_{\text{markings } M} \tilde{G}_M(t_1, \dots, t_V) = 0 \quad (4.5)$$

holds.

Proof. We can assume that the vertices have distinct times, because the distributions (4.4) and the left-hand side of (4.5) do not involve contact terms. Then, there is a lowest

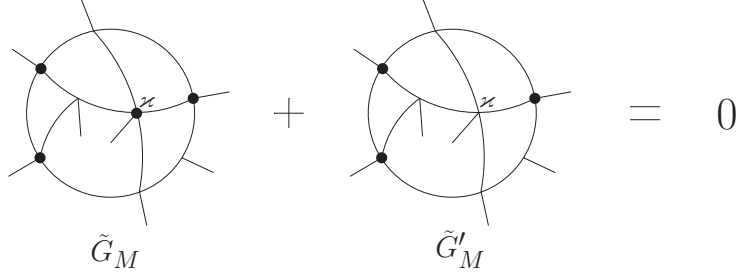


Figure 6: Mutually canceling contributions

time, which we denote by t_0 . Let \varkappa denote its vertex. Formula (4.5) holds, because the sum on the left-hand side contains pairs of mutually canceling contributions, as shown in fig. 6. Specifically, for every diagram G_M that has \varkappa unmarked, there is an almost identical diagram G'_M that differs from G_M just for the marking of \varkappa . The contribution \tilde{G}'_M due to G'_M is opposite to the contribution \tilde{G}_M due to G_M , because the extra marking implies an extra minus sign. On the other hand, all the propagators of G_M and G'_M have equal values. Those that do not involve \varkappa coincide, because they connect the same vertices. Those that involve \varkappa coincide, because the scheme (4.4) implies

$$\begin{aligned}
 (\varkappa l_j \nu_b) &\rightarrow -ie^{i(t_0-t_b)\zeta_j^-}, & (\varkappa l_j \hat{\nu}_b) &\rightarrow -ie^{i(t_0-t_b)\xi_j^-}, \\
 (\hat{\varkappa} l_j \nu_b) &\rightarrow -ie^{i(t_0-t_b)\zeta_j^-}, & (\hat{\varkappa} l_j \hat{\nu}_b) &\rightarrow -ie^{i(t_0-t_b)\xi_j^-}, \\
 (\nu_a l_j \varkappa) &\rightarrow ie^{i(t_a-t_0)\zeta_j^+}, & (\hat{\nu}_a l_j \varkappa) &\rightarrow ie^{i(t_a-t_0)\xi_j^+}, \\
 (\nu_a l_j \hat{\varkappa}) &\rightarrow ie^{i(t_a-t_0)\zeta_j^+}, & (\hat{\nu}_a l_j \hat{\varkappa}) &\rightarrow ie^{i(t_a-t_0)\xi_j^+},
 \end{aligned}$$

which shows that in all cases a marked \varkappa gives the same propagator as does an unmarked \varkappa . \square

The next step is to extract useful pieces of information from the result (4.5). The left-hand side of equation (3.6) can be expanded as a sum

$$\sum_{\text{markings } M} (-1)^m \prod_{i=1}^I p_{Mi}(E_i) = \sum_{\theta} c_{\theta} \prod_{i=1}^I \frac{1}{E_i - \theta_i} \quad (4.6)$$

of polar monomials

$$\prod_{i=1}^I \frac{1}{E_i - \theta_i}, \quad (4.7)$$

where θ is an assignment of polar numbers $\theta_i = \zeta_i^+, \xi_i^+, \zeta_i^-$ or ξ_i^- to the legs ℓ_i of the diagram

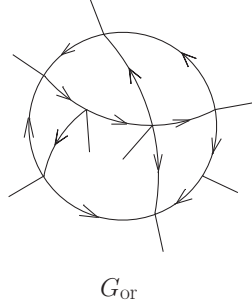


Figure 7: Diagram with time ordered legs

and c_θ are numerical coefficients. When we integrate on the loop energies,

$$\sum_{\theta} c_\theta \int \prod_{i=1}^I \frac{1}{E_i - \theta_i} \prod_{j=1}^L \frac{de_j}{2\pi}, \quad (4.8)$$

multiply by $(2\pi)\delta(\sum_{i=1}^V \mathcal{E}_i)$ and take the Fourier transform, we get the left-hand side of (4.5). If we make these operations on a single polar monomial (4.7), we obtain a contribution that is proportional to a product of θ functions times various exponential factors. We schematically write it as

$$\prod_{j=1}^I \theta(\Delta t_j) e^{i\rho_j \Delta t_j} = \Theta(t_1, \dots, t_I) \prod_{j=1}^I e^{i\rho_j \Delta t_j}, \quad \text{where} \quad \Theta(t_1, \dots, t_I) \equiv \prod_{j=1}^I \theta(\Delta t_j). \quad (4.9)$$

Here ρ_j can be ζ_j^+ , ξ_j^+ , $-\zeta_j^-$ or $-\xi_j^-$, and $\Delta t_j = t_{a_j} - t_{b_j}$ in the first two cases, $\Delta t_j = t_{b_j} - t_{a_j}$ in the other two. Note that each product of exponential factors is associated with a unique distribution $\Theta(t_1, \dots, t_I)$.

We start from the knowledge that the left-hand side of (4.5) vanishes. We can isolate each contribution (4.9) from the others by looking at the exponential factors. Since the numbers ζ_j^+ , ξ_j^+ , ζ_j^- and ξ_j^- can be chosen arbitrarily, apart from the signs of their imaginary parts, each contribution (4.9) must disappear independently from equation (4.5).

The Fourier transform (4.9) of a polar monomial can disappear from (4.5) for two reasons: the numerical coefficient c_θ in front of it vanishes, or the distribution $\Theta(t_1, \dots, t_I)$ is identically equal to zero. Consequently, the right-hand side of (3.6) can only contain the polar monomials that have a vanishing $\Theta(t_1, \dots, t_I)$. Thus, it is mandatory to understand when that happens.

Consider the distribution $\Theta(t_1, \dots, t_I)$ together with the “naked” diagram G , that is to say the diagram G with no markings on the vertices and no orientations on the lines. We want to use $\Theta(t_1, \dots, t_I)$ to equip G with a *time ordering* (which has nothing to do with

the orientation based on the energy flow met so far). Precisely, we equip each G internal line with an arrow pointing from the endpoint of lower time to the endpoint of larger time. Denote the diagram obtained this way by G_{or} (see fig. 7) and its distribution $\Theta(t_1, \dots, t_I)$ by $\Theta(G_{\text{or}})$.

We say that a curve γ is time ordered if its lines have coherent time orientations. We denote the product of the theta functions associated with its lines by $\Theta(\gamma)$.

If γ is not time ordered and t_a, t_b are the times associated with its endpoints, $\Theta(\gamma)$ is nontrivial both for $t_a > t_b$ and $t_a < t_b$. To see this, observe that, since we are just interested in the endpoints, two adjacent lines with coherent time orderings can be collapsed onto a single line with the same ordering. Thus, it is sufficient to consider the cases where adjacent legs have opposite time orderings, as in the examples of fig. 8, where time is the vertical coordinate. It is evident that for arbitrary t_a and t_b , there exist configurations of the intermediate vertices that make $\Theta(\gamma)$ nontrivial.

Now we prove two useful lemmas. The first one is a generalization of the property just shown.

Lemma 2 *Let ν_a and ν_b denote two distinct vertices of G_{or} . Denote their times by t_a and t_b , respectively. Assume that $\Theta(G_{\text{or}})$ is nontrivial, but vanishes identically for $t_a > t_b$. Then G_{or} contains a time ordered curve that connects ν_a to ν_b .*

Proof. The distribution $\Theta(G_{\text{or}})$ can be viewed as a set constraints on the relative times of the nearest neighbors. When any of those constraints is violated, $\Theta(G_{\text{or}})$ vanishes. We can assume that ν_a and ν_b are not nearest neighbors, because in that case the theorem is trivial. Assume that $\Theta(G_{\text{or}})$ forces a vertex ν , different from ν_a and ν_b , to be in the future of all its nearest neighbors. If so, send ν to the infinite future, which is equivalent to dropping ν and cutting the legs attached to it. Similarly, if $\Theta(G_{\text{or}})$ forces a vertex $\bar{\nu} \neq \nu_a, \nu_b$ to be in the past of all its nearest neighbors, send it to the infinite past. Once both types of vertices are dropped, a reduced diagram G'_{or} is obtained, equipped with a reduced distribution $\Theta(G'_{\text{or}})$. Since $\Theta(G_{\text{or}})$ vanishes identically for $t_a > t_b$, $\Theta(G'_{\text{or}})$ satisfies the same property. Next,



Figure 8: Adjacent legs with opposite time orderings

repeat the procedure on G'_{or} : $\Theta(G'_{\text{or}})$ may force other vertices, different from ν_a and ν_b , to be in the past or future of all their nearest neighbors; if we drop them, we obtain a further reduced diagram G''_{or} , on which we can iterate again. At the end, we remain with a reduced diagram $G_{\text{or}}^{\text{red}}$ that contains ν_a , ν_b and possibly vertices that are forced to have both past and future nearest neighbors. Moreover, $\Theta(G_{\text{or}}^{\text{red}})$ vanishes identically for $t_a > t_b$. In particular, $G_{\text{or}}^{\text{red}}$ cannot contain just ν_a and ν_b , because in that case the distribution $\Theta(G_{\text{or}}^{\text{red}})$ would be identically one. We infer that $G_{\text{or}}^{\text{red}}$ must contain at least one vertex ν besides ν_a and ν_b . Then, ν must have a future neighbor ν_f and a past neighbor ν_p . Similarly, ν_f must have a future neighbor ν'_f , while ν_p must have a past neighbor ν'_p . Continuing like this, we eventually reach ν_b in the future and ν_a in the past, and identify a time ordered curve γ_{ab} that connects ν_a to ν_b . \square

Lemma 3 *The distribution $\Theta(G_{\text{or}})$ is trivial if and only if G_{or} contains a time ordered loop.*

For example, the diagram of fig. 7 has a time ordered loop. A time ordered loop clearly vanishes, because the theta functions conflict with one another, as in

$$\theta(t_1 - t_2)\theta(t_2 - t_1), \quad \theta(t_1 - t_2)\theta(t_2 - t_3)\theta(t_3 - t_1). \quad (4.10)$$

The key content of the Lemma is that this is the only situation that can make $\Theta(t_1, \dots, t_I)$ vanish.

Proof. Assume that G_{or} is a tree diagram. Then, the distribution $\Theta(G_{\text{or}})$ is nontrivial, because it just orders the vertices according to time: the configurations t_1, \dots, t_I where $\Theta(t_1, \dots, t_I)$ is equal to one have nonvanishing measure.

Now, proceed by induction. Assume that the theorem holds for diagrams with L loops or less. Consider an $(L+1)$ -loop diagram G_{or} . Cut one leg $(\nu_a \bar{\ell} \nu_b)$, so as to obtain an L loop diagram G_L , which satisfies the theorem by the inductive assumption. If $\Theta(G_L)$ is trivial, it has a time oriented loop and so does $\Theta(G_{\text{or}})$. If $\Theta(G_L)$ is nontrivial, we distinguish two cases: (i) $\Theta(G_L)$ is nontrivial for both $t_a < t_b$ and $t_a > t_b$; (ii) $\Theta(G_L)$ is trivial for either $t_a < t_b$ or $t_a > t_b$. When we close the $(L+1)$ -th loop, the leg $(\nu_a \bar{\ell} \nu_b)$ orders the times t_a and t_b . In case (i), $\Theta(G_{\text{or}})$ is nontrivial. In case (ii), $\Theta(G_{\text{or}})$ is trivial if and only if the time ordering due to $(\nu_a \bar{\ell} \nu_b)$ conflicts with the one due to $\Theta(G_L)$. By Lemma 2, G_L contains a time ordered curve γ_{ab} connecting ν_a and ν_b . Thus, $\Theta(G_{\text{or}})$ is trivial if and only if the union of $(\nu_a \bar{\ell} \nu_b)$ and γ_{ab} is a time oriented loop. \square

Now, let us go back to equation (4.6), that is to say the expansion of the left-hand side of (3.6) in terms of polar monomials (4.7). We recall that every polar monomial leads to a

contribution (4.9), when we integrate on the loop energies and take the Fourier transform. Since each contribution (4.9) is independent of the others, equation (4.5) implies that every time the distribution $\Theta(t_1, \dots, t_I)$ is nontrivial, the coefficient c_θ must vanish. Thus, the right-hand side of (4.6) contains only the polar monomials (4.7) that lead to a trivial $\Theta(t_1, \dots, t_I)$. Moreover, we have just proved that $\Theta(t_1, \dots, t_I)$ is trivial if and only if G_{or} contains a time ordered loop γ_{or} , i.e. $\Theta(\gamma_{\text{or}})$ is trivial. Now we have to understand how this requirement reflects on the polar monomial (4.7).

Consider the legs ℓ_i of γ_{or} and collect the values of their indices i into the set s_{or} . Multiply $\Theta(\gamma_{\text{or}})$ by the appropriate exponential factors $e^{i\rho_j \Delta t_j}$, as in (4.9),

$$\Theta(\gamma_{\text{or}}) \prod_{j \in s_{\text{or}}} e^{i\rho_j \Delta t_j} = \prod_{j \in s_{\text{or}}} \theta(\Delta t_j) e^{i\rho_j \Delta t_j}. \quad (4.11)$$

We first assume that γ_{or} is also oriented, in the sense of the energy flow. Then, the triviality of the distribution (4.11) leads, after Fourier transform, to the identity

$$\int_{-\infty}^{+\infty} \frac{de}{2\pi} \prod_{i \in s_{\text{or}}} \frac{1}{E_i - \theta_i} = 0, \quad (4.12)$$

for arbitrary values of ζ_i^+ , ζ_i^- , ξ_i^+ and ξ_i^- , $i \in s_{\text{or}}$, where e is the loop energy of γ_{or} . Here, e is one of the loop energies e_1, \dots, e_L and appears inside each E_i of (4.12) with coefficient +1.

Now we show that the identity (4.12) holds if and only if the polar numbers θ_i are all placed on the same side with respect to the real axis, which means that the loop γ_{or} is polarized. It is obvious that this condition is sufficient, because if we close the integration path on the half plane with no poles, the residue theorem gives zero. The condition is also necessary, as we show by reductio ad absurdum. Assume that the integral of (4.12) is identically zero when one or more poles are above the real axis and one or more poles are below it. Move all the poles with positive imaginary parts into a single pole θ^+ and all those with negative imaginary parts into a single pole θ^- . This gives an integral of the form

$$\int_{-\infty}^{+\infty} \frac{1}{(e - \theta^+)^{n_+} (e - \theta^-)^{n_-}} \frac{de}{2\pi} = \binom{n_+ + n_- - 2}{n_+ - 1} \frac{i(-1)^{n_+ + 1}}{(\theta^+ - \theta^-)^{n_+ + n_- - 1}},$$

which is obviously nonvanishing, contradicting the assumption. Thus, γ_{or} is polarized.

If γ_{or} is not oriented in the sense of the energy flow, its loop energy e must be defined anew, since it is not one of the standard integrations variables e_1, \dots, e_L we have been using so far. Choose a direction for the e flow along γ_{or} and split the set s_{or} into $s'_{\text{or}} \cup s''_{\text{or}}$, such that the legs ℓ_i with $i \in s'_{\text{or}}$ have orientations coherent with the e flow, while the legs ℓ_i with $i \in s''_{\text{or}}$ have orientations opposite to the e flow. Consider the integrand of (4.12) and write

$E_i = e + E'_i$ for $i \in s'_{\text{or}}$, $E_i = -e + E'_i$ for $i \in s''_{\text{or}}$, where E'_i are energies independent of e . Then, the condition that the Fourier transform of (4.11) vanishes identically gives

$$\int_{-\infty}^{+\infty} \frac{de}{2\pi} \prod_{i \in s'_{\text{or}}} \frac{1}{E'_i + e - \theta_i} \prod_{j \in s''_{\text{or}}} \frac{1}{E'_j - e - \theta_j} = 0.$$

We know that this condition holds if and only if the poles are located on the same side of the complex plane with respect to the real e axis. This means that each θ_i with $i \in s'_{\text{or}}$ must be located on one half plane and each θ_i with $i \in s''_{\text{or}}$ must be located on the other half plane. We see again that the loop γ_{or} is polarized, i.e. adjacent γ_{or} legs of coherent (opposite) orientations carry polar numbers of coherent (opposite) polarities.

Since the conclusions hold for arbitrary energies, as well as arbitrary polar numbers ζ_i^+ , ξ_i^+ , ζ_i^- and ξ_i^- , it also holds for arbitrary polar numbers σ_i^+ , τ_i^+ , σ_i^- and τ_i^- . This gives formula (3.6) and concludes the proof. \square

5 Examples and applications

In quantum field theory, we can decompose each propagator into the sum of two polar numbers, called “half propagators”, each of which has a unique pole. The polarity refers to the location of the pole with respect to the real axis. From now on, positive (negative) polarity means that the pole is located below (above) the real axis.

A polarized monomial has a polarized loop. As explained above, the integral on the energy of a polarized loop is equal to zero, because all the poles of its integrand are located on the same side with respect to the real axis. Therefore, the integral of the left-hand side of (3.6) on the loop momenta vanishes. This operation leads to the diagrammatic cutting equation associated with the diagram G .

In this section, we illustrate these properties in various one-loop and two-loop diagrams and include the algebraic identities of other diagrams, up to three loops. In section 6 we generalize them to prove the perturbative unitarity of quantum field theories.

5.1 Bubble diagram

The “bubble” diagram is the diagram (b) of fig. 1. Its marked versions are shown in fig. 3 and lead to the polynomial identity (3.7). Now we show how to apply this identity and derive the diagrammatic cutting equations.

The value of the bubble diagram is given by the convolution of two propagators. In D

dimensional scalar field theories, we have

$$\mathcal{B} = \int \frac{d^D k}{(2\pi)^D} \frac{1}{k^2 - m_1^2 + i\epsilon} \frac{1}{(k-p)^2 - m_2^2 + i\epsilon'}. \quad (5.1)$$

For convenience, we keep the infinitesimal widths ϵ and ϵ' different from each other. The reason will become apparent below. The arguments that follow focus on the energy integral, which is convergent. We do not need to pay attention to the integral on the space momentum. That integral may diverge in certain dimensions D , in which case it can be defined by means of a regularization (the dimensional technique being the most convenient choice).

Define the polar numbers

$$\sigma_1^\pm = \pm \frac{1}{2\omega_{1\epsilon}} \frac{1}{k^0 \mp \omega_{1\epsilon}}, \quad \sigma_2^\pm = \pm \frac{1}{2\omega_{2\epsilon'}} \frac{1}{k^0 - p^0 \mp \omega_{2\epsilon'}}, \quad \tau_i^\pm = -(\sigma_i^\mp)^*, \quad (5.2)$$

where the complex frequencies are $\omega_{1\epsilon} = \sqrt{\mathbf{k}^2 + m_1^2 - i\epsilon}$, $\omega_{2\epsilon'} = \sqrt{(\mathbf{k} - \mathbf{p})^2 + m_2^2 - i\epsilon'}$ and contain the ϵ, ϵ' prescriptions. We see that σ_i^+ and τ_i^+ have poles located below the real axis, while σ_i^- and τ_i^- have poles located above the real axis.

Note that the definition of polarity we use here differs from the one used in the proof of the previous section in several respects. In particular, the signs of the imaginary parts of σ_i^\pm and τ_i^\pm do not agree with the signs of the imaginary parts of their poles. We recall that the algebraic theorem of section 3 works with any definition of polarity.

The combinations

$$z_1 = \sigma_1^+ + \sigma_1^- = \frac{1}{k^2 - m_1^2 + i\epsilon}, \quad z_2 = \sigma_2^+ + \sigma_2^- = \frac{1}{(k-p)^2 - m_2^2 + i\epsilon'}, \quad w_i = -z_i^*, \quad (5.3)$$

give the propagators and (minus) their conjugates.

Now, define the ‘‘cut propagators’’ u_i and v_i as

$$u_i = \sigma_i^+ + \tau_i^-, \quad v_i = \sigma_i^- + \tau_i^+. \quad (5.4)$$

We call these combinations cut propagators even if they are defined at $\epsilon, \epsilon' \neq 0$. Strictly speaking, the usual cut propagators are obtained in the limits $\epsilon, \epsilon' \rightarrow 0$. For example, using $\omega_{1\epsilon} \sim \omega_1 - i\epsilon/(2\omega_1)$, where $\omega_1 = \omega_{1\epsilon}|_{\epsilon=0}$, we get

$$\lim_{\epsilon \rightarrow 0} u_1 = -2i\pi\theta(k^0)\delta(k^2 - m_1^2), \quad \lim_{\epsilon \rightarrow 0} v_1 = -2i\pi\theta(-k^0)\delta(k^2 - m_1^2), \quad (5.5)$$

which are the usual cut propagators of a scalar field, multiplied by $-i$. The limits of u_2 and v_2 for $\epsilon' \rightarrow 0$ give (5.5) with the replacements $k \rightarrow k - p$ and $m_1 \rightarrow m_2$.

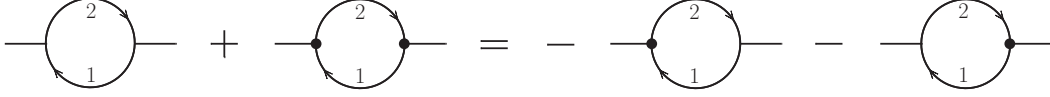


Figure 9: Cutting equation of the bubble diagram

At this point, we can write the bubble diagram (5.1) and its conjugate in the form

$$\mathcal{B} = \int z_1 z_2, \quad \mathcal{B}^* = \int w_1 w_2,$$

and use the polynomial identity (3.7). The decomposition (3.7) is advantageous for the integration over the loop energy k^0 . Expand the right-hand side of (3.7) as a sum of polarized monomials and pick one such monomial at a time. Its poles are located on the same side of the complex plane with respect to the real axis. When we integrate k^0 along the real axis, we can close the integration path at infinity on the side that contains no poles. By the residue theorem, each polarized monomial gives zero. Thus, the momentum integral of the left-hand side of (3.7) also vanishes. This gives the relation

$$\mathcal{B} + \mathcal{B}^* = \int u_1 v_2 + \int v_1 u_2, \tag{5.6}$$

which is graphically shown in fig. 9. The Feynman rules are those of fig. 2 (together with a factor -1 for every marked vertex).

The right-hand side of fig. 9 is minus the sum of the cut diagrams, which is popularly represented as shown in fig. 10 by shadowing the areas that contain the marked vertices.

Note that ϵ, ϵ' are still different from zero, so the identity (5.6) is actually more general than the ones we are accustomed to in quantum field theory. Indeed, in those identities, the cut propagators u_i are replaced by their limits (5.5). In our identity, instead, ϵ and ϵ' can be arbitrary positive numbers.

We see that the diagrammatic cutting equation of fig. 9 is a straightforward consequence of the simple polynomial identity (3.7).

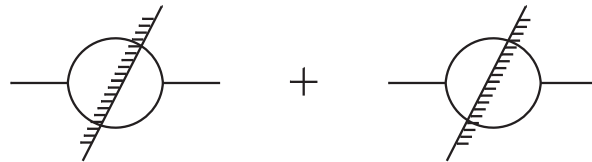


Figure 10: Cut bubble diagrams

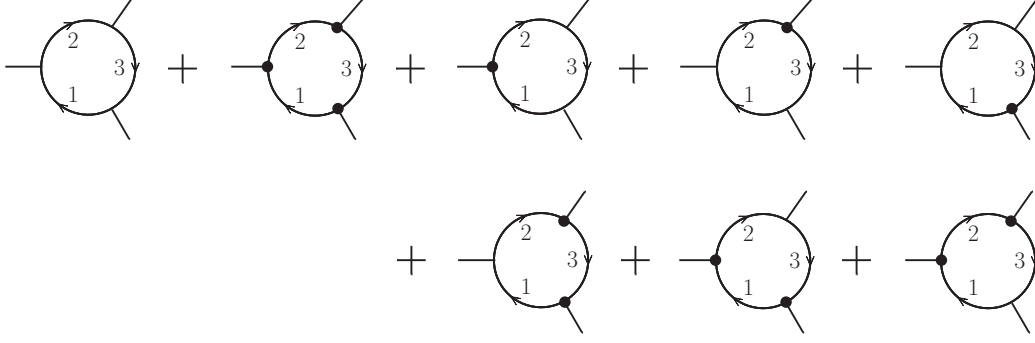


Figure 11: Marked triangle diagrams

5.2 Triangle and box diagrams

The “triangle” diagram is the one-loop oriented diagram with three adjacent lines. It leads to the polynomial identity

$$\begin{aligned}
 z_1 z_2 z_3 - w_1 w_2 w_3 - u_1 v_2 z_3 - z_1 u_2 v_3 - v_1 z_2 u_3 + v_1 u_2 w_3 + w_1 v_2 u_3 + u_1 w_2 v_3 \\
 = \prod_{i=1}^3 (\sigma_i^+ - \tau_i^+) + \prod_{i=1}^3 (\sigma_i^- - \tau_i^-),
 \end{aligned} \tag{5.7}$$

which is easy to verify directly. The left-hand side of this formula can be worked out from the sum of the triangle diagram plus its marked versions, shown in fig. 11, by applying the Feynman rules of fig. 2 and multiplying by $(-1)^m$, where m is the number of marked vertices. The right-hand side of (5.7) corresponds of the polynomial \mathcal{P}_G of formula (3.6), which in the one-loop case is known in closed form due to formula (3.8).

The triangle diagram gives the integral

$$\mathcal{J} = \int \frac{d^D k}{(2\pi)^D} \frac{1}{k^2 - m_1^2 + i\epsilon} \frac{1}{(k-p)^2 - m_2^2 + i\epsilon'} \frac{1}{(k-q)^2 - m_3^2 + i\epsilon''}, \tag{5.8}$$

where p and q are external momenta. To extend the analysis of the previous section, we add the definitions

$$\begin{aligned}
 \sigma_3^\pm &= \pm \frac{1}{2\omega_{3\epsilon''}} \frac{1}{k^0 - q^0 \mp \omega_{3\epsilon''}}, & z_3 &= \sigma_3^+ + \sigma_3^-, & \tau_3^\pm &= -(\sigma_3^\mp)^*, & w_3 &= -z_3^*, \\
 u_3 &= \sigma_3^+ + \tau_3^-, & v_3 &= \sigma_3^- + \tau_3^+,
 \end{aligned} \tag{5.9}$$

to the previous ones, where $\omega_{3\epsilon''} = \sqrt{(\mathbf{k} - \mathbf{q})^2 + m_3^2 - i\epsilon''}$.

Again, we integrate both members of equation (5.7) on k^0 . The right-hand side gives zero by the residue theorem, because of our definition of polarity, while the left-hand side

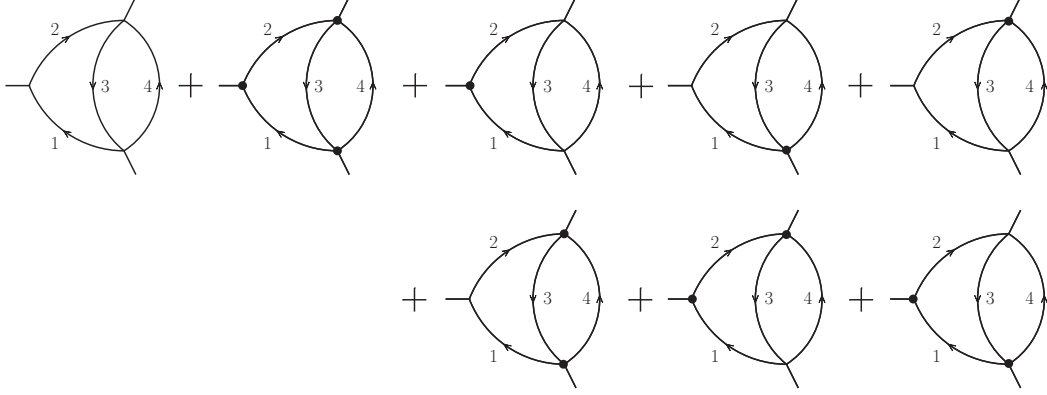


Figure 12: Marked chestnut diagrams

leads to the identity

$$\mathcal{T} + \mathcal{T}^* - \int u_1 v_2 z_3 - \int z_1 u_2 v_3 - \int v_1 z_2 u_3 + \int v_1 u_2 w_3 + \int w_1 v_2 u_3 + \int u_1 w_2 v_3 = 0.$$

This formula is graphically represented by equating the sum of fig. 11 to zero. It can also be viewed as a diagrammatic cutting equation, by shadowing the marked areas of the diagrams. Once again, the diagrammatic cutting equation is rooted into the simple polynomial identity (5.7).

Without giving further details, we report the polynomial identity associated with the box diagram, which is

$$\begin{aligned} & z_1 z_2 z_3 z_4 + w_1 w_2 w_3 w_4 - u_1 v_2 z_3 z_4 + u_1 w_2 v_3 z_4 - u_1 w_2 w_3 v_4 - z_1 u_2 v_3 z_4 + z_1 u_2 w_3 v_4 - v_1 u_2 w_3 w_4 \\ & - z_1 z_2 u_3 v_4 + v_1 z_2 u_3 w_4 - w_1 v_2 u_3 w_4 - v_1 z_2 z_3 u_4 + w_1 v_2 z_3 u_4 - w_1 w_2 v_3 u_4 + v_1 u_2 v_3 u_4 + u_1 v_2 u_3 v_4 \\ & = \prod_{i=1}^4 (\sigma_i^+ - \tau_i^+) + \prod_{i=1}^4 (\sigma_i^- - \tau_i^-). \end{aligned}$$

5.3 Two-loop and three-loop diagrams

Now we give a two-loop example, the chestnut diagram shown as first in fig. 12, which includes its marked versions. The associated polynomial identity reads

$$\begin{aligned} & z_1 z_2 z_3 z_4 - w_1 w_2 w_3 w_4 - u_1 v_2 z_3 z_4 - v_1 z_2 u_3 v_4 - z_1 u_2 v_3 u_4 + v_1 u_2 w_3 w_4 + u_1 w_2 v_3 u_4 + w_1 v_2 u_3 v_4 \\ & = \sum [a \rho_1^+ \rho_2^+ \rho_3^+ \eta_4 + b \rho_1^- \rho_2^- \rho_3^- \eta_4 + c \eta_1 \eta_2 \rho_3^+ \rho_4^+ + d \eta_1 \eta_2 \rho_3^- \rho_4^-], \quad (5.10) \end{aligned}$$

where each ρ_i can stand for σ_i or τ_i and each η_i can stand for σ_i^+ , σ_i^- , τ_i^+ or τ_i^- . The sum is over all such choices, a, b, c, d denoting unspecified numerical coefficients.

The oriented loops are 123 and 34. The loop 124 is redundant, because whenever it is polarized, either 123 or 34 is also polarized. The right-hand side of (5.10) is a sum of polarized monomials that factorize the polarized loops $\rho_1^+ \rho_2^+ \rho_3^+$, $\rho_1^- \rho_2^- \rho_3^-$, $\rho_3^+ \rho_4^+$ or $\rho_3^- \rho_4^-$, as required by formula (3.6).

The chestnut diagram gives the loop integral

$$\mathcal{C} = \int d\mu \frac{1}{k^2 - m_1^2 + i\epsilon_1} \frac{1}{(k-p)^2 - m_2^2 + i\epsilon_2} \frac{1}{(k+q-p')^2 - m_3^2 + i\epsilon_3} \frac{1}{q^2 - m_4^2 + i\epsilon_4},$$

where p and p' are external momenta and the measure $d\mu$ is $d^D k d^D q / (2\pi)^{2D}$. The definitions of polar numbers, propagators and cut propagators are straightforward, mimicking the formulas (5.2), (5.3), (5.4) and (5.9). When we integrate on the loop momenta, the right-hand side of (5.10) gives zero, since every term contains a polarized oriented loop. The integral on the energy of that loop vanishes by the residue theorem, since the integrand has poles only above or below the real axis. In the end, we obtain the diagrammatic cutting equation graphically represented by equating the sum of fig. 12 to zero.

If we flip the orientations of the legs 3 and 4, we obtain a different orientation, for the diagram, and a different polynomial identity, which is equal to (5.10) upon exchange of the subscripts 3 and 4. In that case, the oriented loops become 124 and 34, so the right-hand side of (5.10) contains the polarized factors $\rho_1^+ \rho_2^+ \rho_4^+$, $\rho_1^- \rho_2^- \rho_4^-$, $\rho_3^+ \rho_4^+$ and $\rho_3^- \rho_4^-$. The two orientations lead to equivalent identities for the integral \mathcal{C} , because they amount to send the loop momentum q to $-k - q$. To better see this, it is convenient to switch off the external momenta p and p' , because they are not important for the polynomial identity.

We also report the polynomial identities associated with the two-loop self-energy diagrams of fig. 4. The first diagram gives

$$\begin{aligned} & z_1 z_2 z_3 z_4 z_5 + w_1 w_2 w_3 w_4 w_5 - u_1 v_2 z_3 z_4 z_5 - z_1 u_2 v_3 z_4 u_5 - z_1 z_2 z_3 u_4 v_5 - v_1 z_2 u_3 v_4 z_5 \\ & + u_1 w_2 v_3 z_4 u_5 + u_1 v_2 z_3 u_4 v_5 + w_1 v_2 u_3 v_4 z_5 + v_1 u_2 w_3 v_4 u_5 + z_1 u_2 v_3 u_4 w_5 + v_1 z_2 u_3 w_4 v_5 \\ & - v_1 u_2 w_3 w_4 w_5 - w_1 v_2 u_3 w_4 v_5 - w_1 w_2 w_3 v_4 u_5 - u_1 w_2 v_3 u_4 w_5 \\ & = \sum [a\rho_1^+ \rho_2^+ \rho_3^+ \eta_4 \eta_5 + b\rho_1^- \rho_2^- \rho_3^- \eta_4 \eta_5 + c\eta_1 \eta_2 \rho_3^+ \rho_4^+ \rho_5^+ + d\eta_1 \eta_2 \rho_3^- \rho_4^- \rho_5^-]. \end{aligned} \quad (5.11)$$

The second diagram gives the same identity with $\sigma_4^+ \leftrightarrow \sigma_4^-$, $\tau_4^+ \leftrightarrow \tau_4^-$, $\sigma_5^+ \leftrightarrow \sigma_5^-$, $\tau_5^+ \leftrightarrow \tau_5^-$. In either case, the loop 1245 is redundant, because when it is polarized, either 123 or 345 is polarized. Note that in the second diagram the loop 345 is not oriented and the last two contributions of (5.11) become proportional to the polarized loops $\rho_3^+ \rho_4^- \rho_5^-$ and $\rho_3^- \rho_4^+ \rho_5^+$.

Finally, we give a three-loop example, the box diagram equipped with diagonals. Let 1, 2, 3, 4 label the legs of the box and 5, 6 the diagonals. Define the leg orientations so that

the oriented loops are 1234, 125 and 236. Then the identity

$$\begin{aligned}
 & z_1 z_2 z_3 z_4 z_5 z_6 - u_1 v_2 z_3 z_4 z_5 u_6 + u_1 w_2 v_3 z_4 v_5 u_6 - u_1 w_2 w_3 v_4 v_5 w_6 - z_1 u_2 v_3 z_4 v_5 z_6 + z_1 u_2 w_3 v_4 v_5 v_6 \\
 & - v_1 u_2 w_3 w_4 w_5 v_6 - z_1 z_2 u_3 v_4 z_5 v_6 + v_1 z_2 u_3 w_4 u_5 v_6 - w_1 v_2 u_3 w_4 u_5 w_6 - v_1 z_2 z_3 u_4 u_5 z_6 \\
 & + w_1 v_2 z_3 u_4 u_5 u_6 - w_1 w_2 v_3 u_4 w_5 u_6 + v_1 u_2 v_3 u_4 w_5 z_6 + u_1 v_2 u_3 v_4 z_5 w_6 + w_1 w_2 w_3 w_4 w_5 w_6 \sim 0
 \end{aligned}$$

holds, where the right-hand side of (3.6), which we do not report in full form, is a sum of polarized monomials. The polarized loops are 125, 236, 345 and 146, the last two being nonoriented.

6 Perturbative unitarity of quantum field theories

In this section we show how to use the algebraic cutting equations to prove the perturbative unitarity of quantum field theories. We begin with nonderivative scalar theories. For definiteness, we may consider the φ^4 theory, described by the Lagrangian

$$\mathcal{L} = \frac{1}{2}(\partial_\mu \varphi)(\partial^\mu \varphi) - \frac{m^2}{2}\varphi^2 - \frac{\lambda}{4!}\varphi^4,$$

which is renormalizable in $D \leq 4$. Alternatively, we may take the φ^6 theory, which is renormalizable in $D \leq 3$, or the φ^3 theory, which is renormalizable in $D \leq 6$. The discussion is actually independent of the form of the potential and the number of legs carried by the vertices, as long as they do not contain derivatives. Derivative vertices may be included with a few extra manipulations, which we describe at the end of this section. There, we also generalize the arguments to fields of different spins and nonrenormalizable theories.

Define the polar numbers

$$\sigma_{\mathbf{k}\epsilon}^\pm = \pm \frac{1}{2\omega_{\mathbf{k}\epsilon}} \frac{1}{k^0 \mp \omega_{\mathbf{k}\epsilon}}, \quad \tau_{\mathbf{k}\epsilon}^\pm = -(\sigma_{\mathbf{k}\epsilon}^\mp)^*, \quad (6.1)$$

where $\omega_{\mathbf{k}\epsilon} = \sqrt{\mathbf{k}^2 + m^2 - i\epsilon}$. The poles of $\sigma_{\mathbf{k}\epsilon}^+$, $\tau_{\mathbf{k}\epsilon}^+$ are located below the real axis and those of $\sigma_{\mathbf{k}\epsilon}^-$, $\tau_{\mathbf{k}\epsilon}^-$ are located above the real axis. The combinations

$$z_{\mathbf{k}\epsilon} = \sigma_{\mathbf{k}\epsilon}^+ + \sigma_{\mathbf{k}\epsilon}^- = \frac{1}{k^2 - m^2 + i\epsilon}, \quad w_{\mathbf{k}\epsilon} = -z_{\mathbf{k}\epsilon}^*, \quad u_{\mathbf{k}\epsilon} = \sigma_{\mathbf{k}\epsilon}^+ - (\sigma_{\mathbf{k}\epsilon}^+)^*, \quad v_{\mathbf{k}\epsilon} = \sigma_{\mathbf{k}\epsilon}^- - (\sigma_{\mathbf{k}\epsilon}^-)^*,$$

give the propagators, their conjugates and the cut propagators. As before, we can use a different ϵ for each propagator.

Given a Feynman diagram G with V vertices and I internal legs, we assign loop energies and an orientation to it as specified by proposition 1 of section 2. We can promote the

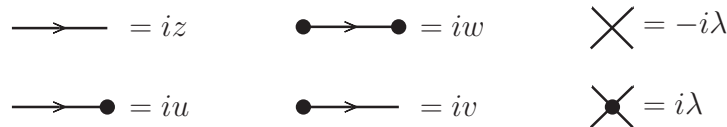


Figure 13: Feynman rules in the standard notation

energy assignments to assignments for the full momenta of the internal legs. So doing, we obtain a parametrization of G in momentum space.

The Feynman rules we have used so far are made of the propagators of fig. 2 plus the rule that an unmarked vertex is equal to $+1$ and a marked vertex is equal to -1 . The Feynman rules commonly used in quantum field theory are slightly different, since they have an extra factor i for each propagator (cut or not) and an extra factor $-i\lambda$ for each vertex (marked or not), λ being the coupling. We show them in fig. 13. Each time we compute a diagram with the rules of the previous sections, we miss the overall factor $i^I(-i\lambda)^V$ with respect to the more common notation of fig. 13. For the rest of this section, we switch to the common notation.

After these redefinitions, the propagator iw connecting two marked points is the complex conjugate of the propagator iz connecting two unmarked points. Moreover, the propagators iu and iv connecting a marked point to an unmarked one are real. Finally, the marked vertices are the complex conjugates of the unmarked vertices.

Now we turn to the identity (3.6) and integrate it on the loop momenta. If G contains no tadpoles, the right-hand side vanishes, because it is a sum of polarized monomials. We recall that a polarized monomial has a polarized loop γ_{pol} . As explained in section 4, we can reparametrize the loop integral so that the energy e of γ_{pol} is one of the integrated variables. The integral on e is zero by the residue theorem, since its integrand has poles only above or below the real axis and we can close the integration path on the half plane that contains no poles. The integral of the left-hand side of (3.6) thus also vanishes, which gives the cutting equation. Once we multiply the identity by the factors $i^{I+V}(-\lambda)^V$ and switch to the notation of fig. 13, we arrive at the common diagrammatic cutting equation

$$G(p_1, \dots, p_n) + \bar{G}(p_1, \dots, p_n) = - \sum_{\text{proper markings } M} G_M(p_1, \dots, p_n), \quad (6.2)$$

where p_1, \dots, p_n are the external momenta, G is the diagram with all unmarked vertices, \bar{G} is the diagram with all marked vertices, and G_M denotes a diagram with a “proper” marking, i.e. with at least one marked vertex and one unmarked vertex.

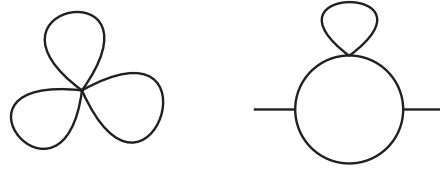


Figure 14: Diagrams with tadpoles

Strictly speaking, (6.2) is the common cutting equation only in the limit $\epsilon \rightarrow 0$, where the cut propagators force the energy to flow from the unmarked endpoints to the marked endpoints. In that limit, numerous marked diagrams vanish due to energy conservation. Those which survive are precisely the usual cut diagrams. Nevertheless, it is always possible to view a marked diagram as a cut diagram by means of closed cuts that circle subdiagrams made of marked vertices. This way, we can extend the common terminology by calling equation (6.2) a cutting equation even at $\epsilon \neq 0$.

There is a caveat, though: we know that the diagrams that contain tadpoles are not covered by the theorem of section 3. Thus, as far as we know now, equation (6.2) only holds for diagrams that contain no tadpoles. We can extend formula (6.2) to the whole set of diagrams as follows.

Tadpoles are loop diagrams with a unique vertex, $V = 1$, so they have as many internal lines as loops, by the topological identity $L - I + V = 1$. A three-loop example of a tadpole and a two-loop example of diagram with a tadpole are shown in fig. 14. We recall that the reason why the diagrams with tadpoles are not covered by the theorem is that tadpoles lead to the integrals of single polar numbers, which are not convergent. Indeed, they behave as $\int dk^0/k^0$ for k^0 large.

Tadpoles and diagrams with tadpoles can be straightforwardly included in the treatment, as long as they satisfy one additional assumption, which we call the *tadpole assumption*: the value of a tadpole with an unmarked vertex must be opposite to the value of its marked version. Graphically, we have fig. 15.

Now we show that the tadpole assumption allows us to derive the cutting equations

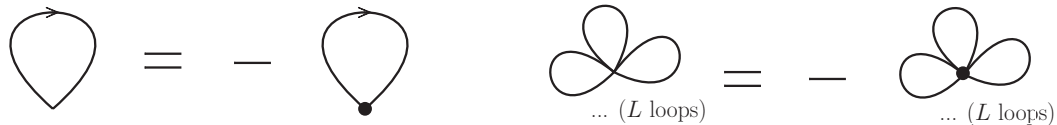


Figure 15: Tadpole assumption

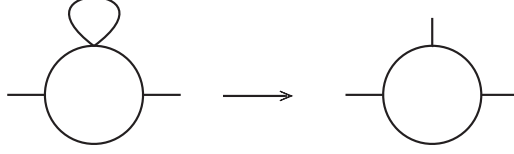


Figure 16: Tadpole assumption

satisfied by the diagrams that contain tadpoles. Consider such a diagram, and call it G_T . If we replace its tadpoles with external legs, we obtain a diagram $G_{\hat{T}}$ that satisfies (6.2).

For example, let G_T denote the second diagram of fig. 14. If we replace the tadpole subdiagram with an external leg, we obtain a diagram $G_{\hat{T}}$ that is equivalent to the triangle diagram treated in the previous section (see fig. 16). We know that $G_{\hat{T}}$ satisfies the identity obtained by equating the sum of fig. 11 to zero, which leads to formula (6.2). Now, take fig. 11 and consider the upper-right external leg and the vertex ν to which it is attached. Suppress that leg and glue the tadpole to the vertex ν . Thanks to the first identity of fig. 15, it does not matter whether ν is marked or not, since the value of the tadpole (neglecting the minus sign due to the marked vertex, because it is already counted inside $G_{\hat{T}}$) in the same in both cases. This means that the tadpole attachment amounts to multiplying the sum of fig. 11 by an overall factor. What we obtain by doing this and equating the total to zero is precisely the cutting equation satisfied by G_T .

The property illustrated in this simple example can be generalized to all tadpole diagrams G_T , as long as the tadpole assumption holds. Ultimately, to derive the cutting equations of tadpole diagrams, it is sufficient to ignore the tadpole subdiagrams and apply the procedure used for every other diagram.

It is easy to check that the scalar theories we are considering satisfy the tadpole assumption, if the dimensional regularization is used and ϵ is sent to zero. For example, the value of the one-loop tadpole is [with the rules of fig. 13]

$$\int \frac{d^D k}{(2\pi)^D} \frac{i(-i\lambda)}{k^2 - m^2 + i\epsilon} = -i\lambda \frac{\Gamma(1 - \frac{D}{2})}{(4\pi)^{D/2}} (m^2 - i\epsilon)^{(D-2)/2} \rightarrow -i\lambda \frac{\Gamma(1 - \frac{D}{2})}{(4\pi)^{D/2}} m^{D-2}, \quad (6.3)$$

while its marked version has the opposite value. The reason is that the marked version carries a minus sign due to the marked vertex and two other minus signs that compensate each other. Recall that the propagator connecting two marked points is $iw = -iz^*$. The conjugation of z flips the sign of the prescription $+i\epsilon$, which leads to a factor -1 that compensates the minus sign in front of iz^* . Thus, the first identity of fig. 15 holds.

The L -loop tadpole is equal to the L -th power of (6.3), divided by $(-i\lambda)^{L-1}$. It satisfies

the second identity of fig. 15, because its marked version carries a minus sign for the marked vertex, while the minus signs coming from the relation $iw = -iz^*$ still compensate each other.

We have proved that, in the end, all Feynman diagrams satisfy the diagrammatic cutting equations (6.2). From this point on, the proof of perturbative unitarity can proceed according to the common strategy [4].

The proof extends to (local) theories with derivative vertices and propagators with non-trivial polynomial numerators. The algebraic cutting equations are the same. The difference is that, before switching to the diagrammatic cutting equations, we must multiply both sides of formula (3.6) by appropriate polynomial numerators. We must show that the right-hand side still vanishes after integrating on the energies. This is less obvious than before.

When the numerator contains enough powers of the energy, contact terms may appear. Contact terms collapse propagators and generate new types of vertices and diagrams, which obey their own cutting equations. As shown in ref. [4], it is possible to associate each diagram G with a set of separate cutting equations that involve no contact terms, the sum of which is equivalent to the G cutting equations at $\epsilon \rightarrow 0$. For this reason, there is no loss of generality in assuming that contact terms are absent. Since the propagators we are considering contain two powers of the energy in the denominators, we can assume that the numerators of the diagram G contain at most one power of each loop energy.

As before, we can restrict to diagrams G with no tadpoles, since tadpoles are easily attached to G at the end. Thus, every polarized loop γ_{pol} that appears in \mathcal{P}_G contains two or more internal legs. If the internal legs are at least three, the energy integral is still convergent: each polar number behaves like $1/E$ for large energy E , while the numerator provides at most one E power; since the integrand of a polarized loop has all the poles on the same side of the integration path, the residue theorem gives zero.

The only case that deserves attention is when the polarized loop γ_{pol} has two legs, and, therefore, two vertices, which we call ν and ν' . We can assume that γ_{pol} is oriented. Due to the nontrivial numerator, we get the integrals

$$\frac{1}{4\omega_1\omega_2} \int_{-\infty}^{+\infty} \frac{dE}{2\pi} \frac{E}{(E - \alpha \pm i\epsilon)(E - \beta \pm i\epsilon')} = \mp \frac{i}{8\omega_1\omega_2}, \quad (6.4)$$

depending on the polar numbers of γ_{pol} , where α and β are real. We have not included the values of the vertices in formula (6.4). We want to show that the contributions (6.4) cancel each other. The reason is that each polarized loop that contributes with the upper sign, i.e. $\gamma_{\text{pol}} = \sigma_1^+ \sigma_2^+, \tau_1^+ \sigma_2^+, \sigma_1^+ \tau_2^+, \tau_1^+ \tau_2^+$, is compensated by a polarized loop that contributes with the lower sign, i.e. $\gamma_{\text{pol}} = \sigma_1^- \sigma_2^-, \tau_1^- \sigma_2^-, \sigma_1^- \tau_2^-, \tau_1^- \tau_2^-$.

Consider the left-hand side of equation (3.6). Isolate the contributions where $\gamma_{\text{pol}} = \sigma_1^+ \sigma_2^+$ and $\gamma_{\text{pol}} = \sigma_1^- \sigma_2^-$. They come from the diagrams G_M where both ν and ν' are unmarked (recall that γ_{pol} is oriented) and the legs of the loop are $z_1 z_2$. Such diagrams compensate each other, when $\epsilon \rightarrow 0$, because the coefficients of $\sigma_1^+ \sigma_2^+$ and $\sigma_1^- \sigma_2^-$ are the same, but the values of the polarized loops are opposite, by formula (6.4). A similar argument applies to the pair $\tau_1^+ \tau_2^+$ and $\tau_1^- \tau_2^-$, which comes from $w_1 w_2$ (with both ν and ν' marked), as well as the pair $\sigma_1^+ \tau_2^+$ and $\tau_1^- \sigma_2^-$, which comes from $u_1 v_2$, and finally the pair $\tau_1^+ \sigma_2^+$ and $\sigma_1^- \tau_2^-$, which comes from $v_1 u_2$. In the last two cases one vertex ν or ν' is marked and the other one is unmarked.

We conclude that the proof of perturbative unitarity based on the algebraic cutting equations applies to all scalar field theories, including those that have derivative vertices, as well as the nonrenormalizable ones. Following the guidelines of ref. [4], the proof can also be generalized to the theories that include fermions, gauge fields and gravity, as long as they are local, Hermitian and their kinetic terms are polynomials of degree two (in the case of bosons) or degree one (in the case of fermions) in the time derivatives.

7 Parity symmetry

Some transformations relate algebraic cutting equations that may look different, but are actually equivalent. Consider the polarity flipping, that is to say the exchanges

$$\sigma_i^+ \longleftrightarrow \sigma_i^-, \quad \tau_i^+ \longleftrightarrow \tau_i^-. \quad (7.1)$$

At the level of the propagators, this operation leaves z_i and w_i invariant and exchanges u_i with v_i . By the Feynman rules of fig. 2, it is equivalent to flip the orientations of all the internal legs of the diagram G . We call (7.1) *parity* transformation.

In the case of one-loop diagrams, the right-hand side \mathcal{P}_G of the identity (3.6) is invariant, by formula (3.8). Consequently, the left-hand side is also invariant. However, this fact may become apparent only after expanding it as a sum of polar monomials. Check for example the identity (5.7), associated with the triangle diagram.

When the number of loops exceeds one, both the left- and right-hand sides of (3.6) may change under the parity transformation. For example, it is easy to check that \mathcal{P}_G does change in the case of the self-energies of fig. 4.

The diagrams G and \bar{G} and so the left-hand side of the diagrammatic cutting equation (6.2) are invariant. For this reason, (7.1) is a symmetry of the diagrammatic cutting equations. Nevertheless, the right-hand side of (6.2) may get organized differently after the transformation.

The algebraic cutting equations likely possess other hidden symmetries that are awaiting to be uncovered. For example, the parity transformation (7.1) can be performed on just one or more legs, instead of all of them. Moreover, the cut and uncut propagators are in some sense dual to each other, because both are linear combinations of half propagators and their different roles only emerge at the graphical level.

8 Conclusions

In this paper, we have proved a set of algebraic identities that provide a clearer understanding of perturbative unitarity in quantum field theory. To conclude, we make some remarks on the virtues of the algebraic approach to perturbative unitarity, in comparison with the usual approach.

When tadpoles are absent, equation (6.2) holds for arbitrary positive values of the widths ϵ of the propagators (6.1). In particular, the widths ϵ need not be infinitesimal. If we choose a different ϵ for each internal leg, our algebraic theorem allows us to keep track of them efficiently throughout the calculation. Each propagator (cut or not) keeps its own ϵ from the beginning to the end and no mixing between the ϵ s of different propagators does occur. This means that we are allowed to freely send them to zero in the order we want. When we do it, the cut propagators become those we are accustomed to, i.e.

$$\lim_{\epsilon \rightarrow 0} iu_{\mathbf{k}\epsilon} = (2\pi)\theta(k^0)\delta(k^2 - m^2), \quad \lim_{\epsilon \rightarrow 0} iv_{\mathbf{k}\epsilon} = (2\pi)\theta(-k^0)\delta(k^2 - m^2).$$

Yet, we stress again that the identity (6.2) also holds when the cut propagators are $iu_{\mathbf{k}\epsilon}$ and $iv_{\mathbf{k}\epsilon}$, where ϵ is arbitrary, at least when tadpoles are absent. When tadpoles are present, the widths can be arbitrary everywhere but in the tadpoles, where they must be set to zero to ensure that the tadpole assumption holds. Similar arguments hold for the contact terms, which lead to formulas such as (6.4), when derivative vertices are present.

If we do not use the algebraic theorem of this paper and make rather natural operations on the integrands, it is easy to generate inconvenient mixings between the ϵ s of different propagators and encounter ill-defined distributions such as [11]

$$\frac{1}{\omega - \omega' - p^0 - i(\epsilon_1 - \epsilon_2)}, \tag{8.1}$$

where $\omega = \sqrt{\mathbf{k}^2 + m_1^2}$ and $\omega' = \sqrt{(\mathbf{k} - \mathbf{p})^2 + m_2^2}$ are some frequencies, p is an external momentum and k is a loop momentum. It is possible to show (see ref. [11] for details) that the ill-defined part of (8.1) ultimately does not contribute. The theorem proved here guides us through the calculations without ever meeting these ill-defined distributions.

Going through the analysis recently made in ref. [4], where the assumptions behind the proof of perturbative unitarity have been relaxed to a minimum, it is possible to realize that the properties just emphasized can also be proved in the usual nonalgebraic approach. However, an approach like the algebraic one, which makes them so apparent, is of great advantage.

The usual approach is also responsible for giving some false impressions. For example, it suggests that the cut propagators must force the energy propagation in a given direction. This is not true, as the validity of (6.2) at arbitrary, nonvanishing widths points out. Again, it is not impossible to show this fact in the usual approach, because the assumption about the energy flow enters the proof only at a later stage [4]. However, the roles of the various ingredients of the proof become much clearer when the algebraic cutting equations are used.

The algebraic approach is useful to prove perturbative unitarity to all orders in theories that have not been reached by more standard techniques, as recently shown in ref. [12] for the Lee-Wick models and the fakeon models.

Acknowledgments

We are grateful to U. Aglietti and M. Piva for useful discussions.

References

- [1] R.E. Cutkosky, Singularities and discontinuities of Feynman amplitudes, J. Math. Phys. 1 (1960) 429;
M. Veltman, Unitarity and causality in a renormalizable field theory with unstable particles, Physica 29 (1963) 186.
- [2] G. 't Hooft, Renormalization of massless Yang-Mills fields, Nucl.Phys. B 33 (1971) 173;
G. 't Hooft, Renormalizable Lagrangians for massive Yang-Mills fields, Nucl. Phys. B 35 (1971) 167.
- [3] See for example, G. Curci and R. Ferrari, An alternative approach to the proof of unitarity for gauge theories, Nuovo Cimento A 35 (1976) 273, and references therein.
- [4] D. Anselmi, Aspects of perturbative unitarity, Phys. Rev. D 94 (2016) 025028, 16A1 Renormalization.com and arXiv:1606.06348 [hep-th].
- [5] G. 't Hooft and M.J. Veltman, *Diagrammar*, report No. CERN-73-09, available at [this link](#).

- [6] T.D. Lee and G.C. Wick, Negative metric and the unitarity of the S-matrix, Nucl. Phys. B 9 (1969) 209;
 T.D. Lee and G.C. Wick, Finite theory of quantum electrodynamics, Phys. Rev. D 2 (1970) 1033;
 R.E. Cutkosky, P.V Landshoff, D.I. Olive, J.C. Polkinghorne, A non-analytic S matrix, Nucl. Phys. B12 (1969) 281.
- [7] B. Grinstein, D. O'Connell, and M.B. Wise, The Lee-Wick standard model, Phys. Rev. D77 (2008) 025012 and arXiv:0704.1845 [hep-ph];
 C.D. Carone and R.F. Lebed, Minimal Lee-Wick extension of the standard model, Phys. Lett. B668 (2008) 221 and arXiv:0806.4555 [hep-ph];
 J.R. Espinosa and B. Grinstein, Ultraviolet properties of the Higgs sector in the Lee-Wick standard model, Phys. Rev. D83 (2011) 075019 and arXiv:1101.5538 [hep-ph];
 C.D. Carone and R.F. Lebed, A higher-derivative Lee-Wick standard model, J. High Energy Phys. 0901 (2009) 043 and arXiv:0811.4150 [hep-ph];
 B. Grinstein and D. O'Connell, One-Loop Renormalization of Lee-Wick Gauge Theory, Phys. Rev. D78 (2008) 105005 and arXiv:0801.4034 [hep-ph];
 C. D. Carone, Higher-derivative Lee-Wick unification, Phys. Lett. B677 (2009) 306 and arXiv:0904.2359 [hep-ph].
- [8] E. Tomboulis, $1/N$ expansion and renormalization in quantum gravity, Phys. Lett. B 70 (1977) 361;
 E. Tomboulis, Renormalizability and asymptotic freedom in quantum gravity, Phys. Lett. B 97 (1980) 77;
 L. Modesto, Super-renormalizable or finite Lee-Wick quantum gravity, Nucl. Phys. B909 (2016) 584 and arXiv:1602.02421 [hep-th];
 I. Shapiro and L. Modesto, Superrenormalizable quantum gravity with complex ghosts, Phys. Lett. B755 (2016) 279 and arXiv:1512.07600 [hep-th].
- [9] D. Anselmi, On the quantum field theory of the gravitational interactions, J. High Energy Phys. 06 (2017) 086, 17A3 Renormalization.com and arXiv:1704.07728 [hep-th].

- [10] D. Anselmi and M. Piva, A new formulation of Lee-Wick quantum field theory, J. High Energy Phys. 06 (2017) 066, 17A1 Renormalization.com and arXiv:1703.04584 [hep-th].
- [11] D. Anselmi and M. Piva, Perturbative unitarity in Lee-Wick quantum field theory, Phys. Rev. D 96 (2017) 045009 and 17A2 Renormalization.com and arXiv:1703.05563 [hep-th].
- [12] D. Anselmi, Fakeons and Lee-Wick models, J. High Energy Phys. 02 (2018) 141, 18A1 Renormalization.com and arXiv:1801.00915 [hep-th].